Development of a Potential Surface for Simulation of Proton and Hydride Transfer Reactions in Solution: Application to NADH Hydride Transfer

M. M. Hurley and Sharon Hammes-Schiffer*

Department of Chemistry and Biochemistry, University of Notre Dame, Notre Dame, Indiana 46556

Received: January 17, 1997; In Final Form: March 26, 1997[⊗]

This paper presents a new augmented molecular mechanical potential that incorporates significant quantum mechanical effects for proton and hydride transfer reactions in solution and in enzymes. The solvent is treated explicitly, specified covalent bonds in the solute are allowed to break and form, and the charge distribution of the solute is allowed to vary smoothly from that of the reactant to that of the product during the reaction. Moreover, in order to incorporate changes in bond order and hybridization, an efficient constraint dynamics method is combined with switching functions to smoothly vary the structure of the complex from the reactant to the product structure during the reaction. This new methodology is applied to model nicotinamide adenine dinucleotide (NADH) hydride transfer reactions, in particular to the oxidation of ethanol by the NAD^+ analog 1-methyl-nicotinamide in acetonitrile and in water. Both *cis* and *trans* orientations of the NADH amide sidearm and both protonated and deprotonated forms of the substrate are studied. The structures and charge distributions of the model complexes are obtained from *ab initio* gas phase geometry optimizations at the Hartree−Fock 6-31G* level and are utilized to parametrize the potential energy surface. Classical free energy curves in both acetonitrile and water are calculated in order to illustrate the solvent effects on the energy gap between the reactant and the product states. The radial distribution functions between the solute and the water molecules together with the orientational distributions of the hydration shell water molecules are also calculated in order to elucidate the nature and extent of hydrogen bonding between the solvent and the solute.

I. Introduction

Nicotinamide adenine dinucleotide (NADH) hydride transfer reactions are essential for many important biological processes. In these reactions, NAD^+ reversibly oxidizes various alcohols to the corresponding aldehydes and ketones, as depicted in Figure 1. Such reactions occur in a number of key redox steps in the metabolic pathway. Moreover, the NADH generated from these reactions plays an important role in oxidative phosphorylation. Thus, the application of computer simulation to elucidate the mechanism of NADH hydride transfer reactions is critical to the understanding of a wide range of important biochemical processes.

The simulation of NADH hydride transfer reactions is particularly challenging for two reasons. The first challenge is that the potential energy surface that describes these reactions must incorporate quantum mechanical effects such as the formation and breaking of bonds and changes in hybridization, bond order, and charge distribution. Standard molecular mechanical (MM) potentials (i.e. standard parametrized analytical functional forms such as those presented in refs 1 and 2) do not incorporate these effects. One way to incorporate quantum mechanical information is to augment the MM potential with parametrized terms of suitable analytical forms (e.g. refs 3 and 4). Another way to incorporate quantum mechanical information is to combine quantum mechanical and molecular mechanical methods (the QM/MM methods), where reacting portions of the system are treated quantum mechanically (using either *ab initio* or semiempirical electronic structure methods), while the remaining portions of the system are treated with standard MM potentials.[5−9]

The second challenge in the simulation of NADH hydride transfer reactions is that the light mass of the transferring hydride leads to quantum dynamical effects such as hydrogen tunneling. Kinetic isotope effect experiments indicate that hydrogen tunneling plays a significant role in NADH hydride transfer reactions in alcohol dehydrogenase enzymes[10,11] and in some model reactions in solution.[12,13] Therefore standard classical molecular dynamics simulations, in which all of the nuclei move classically, are inadequate for describing NADH hydride transfer reactions. Unfortunately, a fully quantum mechanical description is impractical for such large systems. Thus mixed quantum/classical molecular dynamics methods,[14−21] in which the transferring hydrogen atom is treated quantum mechanically while the remaining nuclei are treated classically, are required to incorporate quantum dynamical effects such as hydrogen tunneling in NADH hydride transfer reactions.

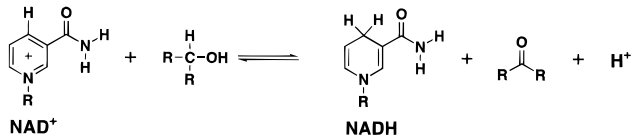

Figure 1. Schematic picture of a general reversible NADH hydride transfer reaction (where R represents a general group and may represent a different group each time it appears).

This paper addresses the first challenge. We have developed a new augmented molecular mechanical potential that incorporates the significant quantum mechanical effects in proton and hydride transfer reactions in solution and in enzymes. The solvent is treated explicitly, specified covalent bonds in the solute are allowed to break and form, and the charge distribution and structure of the solute are allowed to vary during the reaction. This method is designed to be utilized in future mixed quantum/classical molecular dynamics simulations to study the quantum dynamics of proton and hydride transfer. In standard molecular mechanical potentials[1,2] the intramolecular bonds are either constrained or represented by quadratic or Morse poten-

[⊗] Abstract published in *Advance ACS Abstracts,* May 1, 1997.

S1089-5639(97)00269-7 CCC: $14.00

tials (with frequencies determined by factors such as the bond order and the specific atoms involved). Both of these approaches are problematic for NADH hydride transfer because the donor and acceptor carbon atoms change hybridization, leading to significant changes in structure and in bond frequencies. In order to address this problem, we have developed new methodology that incorporates these structural changes by combining an efficient constraint dynamics method with switching functions to smoothly vary the structure of the complex from the reactant to the product structure. This has the advantage of eliminating the intramolecular vibrations, which allows us to use a larger molecular dynamics time step. Switching functions are also used to smoothly vary the atomic charges of the solute from the charge distribution of the reactant to that of the product complex during the reaction. Moreover, a double Morse potential is used to describe the interaction between the transferring hydrogen atom and the donor and acceptor atoms in order to allow the covalent bonds to form and break.[4]

In addition to presenting this new methodology for the potential energy surface, we present the results of the application of these methods to model NADH hydride transfer reactions. We perform *ab initio* gas phase geometry optimizations at the Hartree−Fock 6-31G* level for the model complexes, and we utilize the resulting structures and charge distributions to determine the parameters in the potential energy surface. Then we calculate the classical free energy curves in both aqueous and acetonitrile solution in order to illustrate the relative solvent stabilization of the reactant and product complexes. We also study the nature and extent of hydrogen bond interactions between aqueous solvent and specific atoms in the solute.

A variety of theoretical methods have already been applied to NADH hydride transfer systems. Semiempirical and *ab initio* calculations have been used to determine the structures, charge distributions, and relative energies of reactants, products, and transition states for model NADH hydride transfer reactions in the gas phase.[22−34] These calculations have been useful in determining structural characteristics such as the degree of puckering of the 1,4-dihydronicotinamide ring and the orientation of the 3-amide group in 1,4-dihydronicotinamide. However, such gas phase calculations neglect the effects of the solvent or protein environment, which have been shown to play an important role in proton and hydride transfer reactions.[16] In order to incorporate these effects, semiempirical and *ab initio* calculations including portions of the protein active site have been performed for model NADH hydride transfer reactions.[32−39] In addition, molecular dynamics (MD) calculations using molecular mechanical potentials have been performed on complexes of dehydrogenase enzymes with NAD^+ and various NAD^+ analogs.[33,39,40] All of these calculations have been used to determine structural information about the complexes and to compare the energetics of different possible mechanisms for the enzyme reactions. These methods, however, do not provide dynamical information on the mechanism of hydride transfer.

Several methods have been utilized to study the dynamical aspects of NADH hydride transfer reactions. Bash and co-workers[41] have utilized a QM/MM method[7] to calculate free energy curves for proton transfer from methanol to imidazole and hydride transfer from methoxide to nicotinamide in solution. In these simulations all of the nuclei move according to the classical equations of motion. Kreevoy, Truhlar, and co-workers have studied hydrogen tunneling effects for hydride transfer between a series of NAD^+ analogs.[42,43] They constructed an experimentally based family of potential energy surfaces and calculated reaction rates and kinetic isotope effects using variational transition state theory in conjunction with semiclassical tunneling calculations. Warshel and co-workers combined a quantum dynamical method based on the Feynman path integral formalism with an empirical valence bond QM/MM potential[8,16] to simulate NADH hydride transfer in solution and in lactate dehydrogenase.[44,45]

The methods presented in this paper are complementary to these other methods and will provide further insight into the mechanism of NADH hydride transfer reactions. An outline of this paper is as follows. Section II describes the methods utilized in this paper, including the generalized constraint dynamics method, the new augmented molecular mechanical potential, the methods used to calculate classical free energy curves,[17] and the methods used to study hydrogen bonding between the solvent and solute.[46] Section III presents the results, including the structures and charge distributions of NADH complexes, the classical free energy curves for NADH hydride transfer reactions in solution, and the radial and orientational distribution functions that illustrate hydrogen bonding between the solvent and the NADH complex. Section IV summarizes the methods and results of this paper.

II. Methods

In this section we first describe the generalized RATTLE constraint dynamics method that we have developed for these types of simulations. We then present the specific terms for the general potential energy surface for proton and hydride transfer reactions in solution. This section concludes with a description of the methods used to calculate the classical free energy curves and the radial and orientational distribution functions that illustrate hydrogen bonding between the solvent and solute.

A. Generalized RATTLE Constraint Dynamics. Two standard methods for constraint dynamics are SHAKE[47] (which is based on the Verlet molecular dynamics algorithm) and RATTLE[48] (based on the velocity Verlet algorithm). In both methods a set of undetermined multipliers is used to represent the magnitudes of the forces directed along the bonds required to maintain constant bond lengths. These undetermined multipliers are calculated in an iterative manner, where the coordinates are adjusted to satisfy each constraint in turn until all constraints are satisfied to within a specified tolerance. In SHAKE only the coordinates must satisfy constraint equations, whereas in RATTLE the velocities as well as the coordinates must satisfy constraint equations. This explicit treatment of the velocities facilitates monitoring and adjusting the system energy.

As discussed in ref 49, the standard constraint dynamics algorithms SHAKE and RATTLE are problematic for systems such as linear triatomics and planar rings. Moreover, the use of these algorithms to maintain the rigidity of large molecules consisting of N_a atoms becomes computationally expensive since it requires the solution of $3N_a$ equations of motion subject to $3N_a - 6$ bond constraints. In order to address these problems, ref 49 presents a new constraint dynamics method based on the SHAKE algorithm. The first advantage of this new method is that any rigid molecule can be treated, including linear triatomics and planar rings. The second advantage is that for all values of N_a no more than 12 equations of motion subject to no more than 6 bond constraints must be solved. Thus, this method is computationally tractable for constraining large molecules.

In the new constraint method presented in ref 49, the complex of N_a atoms is divided into N_p primary atoms with $N_p(N_p - 1)/2$ bond constraints σ_{ij} of length d_{ij} and $N_s = N_a - N_p$ secondary atoms linked to the basic structure by $3N_s$ linear constraints $\boldsymbol{\tau}_\alpha$. Note that for a general three-dimensional

molecule, the basic structure can be defined by four noncoplanar atoms connected by six bond constraints. The primary and secondary constraint equations are

$$\sigma_{ij} = |\mathbf{R}_i^{(p)}(t) - \mathbf{R}_j^{(p)}(t)|^2 - d_{ij}^2 = 0 \quad (1)$$

and

$$\boldsymbol{\tau}_\alpha = \sum_{i=1}^{N_p} C_{\alpha i}\mathbf{R}_i^{(p)}(t) - \mathbf{R}_\alpha^{(s)}(t) = 0 \quad (2)$$

where the coordinates (and masses) of the primary and secondary atoms are denoted by $\mathbf{R}_i^{(p)}(t)$ (and $M_i^{(p)}$) and $\mathbf{R}_\alpha^{(s)}(t)$ (and $M_\alpha^{(s)}$), respectively. (Note that the notation includes the dependence of the coordinates on the time t.) Since the secondary coordinates are related to the primary coordinates by eq 2, the equations of motion for the secondary coordinates can be incorporated into the equations of motion for the primary coordinates (i.e. the undetermined multipliers for the secondary constraint equations can be eliminated). Algebraic manipulation of these equations (shown in Appendix A) leads to the following equations of motion for the primary coordinates:

$$M_i^{(p)}\ddot{\mathbf{R}}_i^{(p)}(t) = F_i(t) - \sum_{k=1}^{N_p-1}\sum_{j=k+1}^{N_p} R_{jk}^i(t)\,\lambda_{jk}(t) \quad (3)$$

where λ_{jk} are undetermined multipliers and $F_i(t)$ and $R_{jk}^i(t)$ (given in Appendix A) depend on the primary and secondary coordinates and on the constants $C_{\alpha i}$. The secondary coordinates and their velocities are calculated using eq 2.

As mentioned above, this method was introduced in ref 49 in conjunction with the SHAKE algorithm. We have reformulated this constraint method in conjunction with the RATTLE algorithm to create what we will call the generalized RATTLE method. In our new formulation, the velocity constraints (i.e. the time derivative of the bond constraints)

$$(\mathbf{R}_i^{(p)}(t) - \mathbf{R}_j^{(p)}(t))\cdot(\dot{\mathbf{R}}_i^{(p)}(t) - \dot{\mathbf{R}}_j^{(p)}(t)) = 0 \quad (4)$$

are maintained in addition to the bond constraints. The details of this method are presented in Appendix B. We are applying the generalized RATTLE method to both the solvent and the solute in the systems described below.

B. Potential Energy Surface and Simulation Parameters. This section describes the individual terms in our general expression for the potential energy surface. For generality, the solute is defined to be comprised of one hydrogen atom and two subunits, A and B. In the reactant state, the hydrogen is covalently bonded to an atom denoted by A1 in subunit A, and in the product state the hydrogen is covalently bonded to an atom denoted by B1 in subunit B. Initially we assume that the hydrogen atom is constrained to move in one dimension along the A1−B1 bond axis. (Note that for the reaction shown in Figure 1 A is the alcohol and B is the NAD^+ analog, and both A1 and B1 are carbon atoms.)

The hydrogen-bonding potential for the solute complex is a double Morse form

$$V_{HB} = D_A[1 - \exp^{-\alpha_A(R_{AH}-R_{AH}^{eq})}]^2 + CD_B[1 - \exp^{-\alpha_B(R_{BH}-R_{BH}^{eq})}]^2 \quad (5)$$

where R_{AH} is the distance between atom A1 and the hydrogen atom being transferred and R_{BH} is the distance between atom B1 and the hydrogen atom being transferred. The parameters R_{AH}^{eq} and R_{BH}^{eq} are the equilibrium values of R_{AH} and R_{BH} in the reactant and product states, respectively. D_A and D_B are dissociation energies for these A1−H and B1−H bonds, and α_A and α_B are obtained from the vibrational frequencies of these A1−H and B1−H bond stretches. The parameter C is chosen to reproduce the energy gap between the reactant and product states in the gas phase. This double Morse function has been shown to describe hydrogen-bonding interactions accurately for a range of systems.[4]

In order to accurately model the electrostatic interactions, the charges on the atoms of the complex must vary as the hydrogen atom is transferred. The charges $q_i^{reactant}$ and $q_i^{product}$ for each atom i in the reactant and product states can be calculated using a charge analysis algorithm such as CHELPG.[50] As the hydrogen atom is transferred, the charges q_i vary smoothly according to the switching function[21]

$$q_i = 0.5[q_i^{reactant}(1 - \tanh(r/a)) + q_i^{product}(1 + \tanh(r/a))] \quad (6)$$

where r is the position of the hydrogen atom relative to a specified point along the A1−B1 bond axis (typically the midpoint or position of the transition state) and a is a flexible parameter chosen to properly mimic charges and bond lengths in the reactant and product states. Recall that the hydrogen atom is constrained to move along the A1−B1 bond axis. For our initial applications we are assuming that the charges are centered on the nuclei, and we are neglecting polarization effects. We have used a value of $a = 0.100$ Å.

The solvent is modeled as a collection of rigid molecules with periodic boundary conditions. The structural constraints on the solvent are maintained using the generalized RATTLE constraint dynamics method described above. The solvent−solvent and solvent−solute nonbonding interactions include site−site Lennard-Jones and Coulomb interactions:

$$V_{LJC} = \sum_{i,j}\left(\frac{q_i q_j}{R_{ij}} + \frac{A_{ij}}{R_{ij}^{12}} - \frac{C_{ij}}{R_{ij}^{6}}\right) \quad (7)$$

where q_i is the charge on site i, R_{ij} is the distance between sites i and j, and the Lennard-Jones parameters for a pair of sites i and j are defined as $A_{ij} = (A_iA_j)^{1/2}$ and $C_{ij} = (C_iC_j)^{1/2}$, where A_i and C_i are the Lennard-Jones parameters associated with site i.

For the solute, we have developed a method that allows the structure to change during the reaction. This method requires that we first obtain the values for the constraint parameters, as defined in eqs 1 and 2, for the reactant ($d_{ij}^{reactant}$ and $C_{\alpha i}^{reactant}$) and the product ($d_{ij}^{product}$ and $C_{\alpha i}^{product}$) states. Typically these parameters are obtained from structures determined from gas phase *ab initio* quantum mechanical calculations. In order to describe the structural changes that occur during the reaction, we use the same switching function for the constraint parameters as is used for the charges (eq 6). Thus,

$$d_{ij} = 0.5[d_{ij}^{reactant}(1 - \tanh(r/a)) + d_{ij}^{product}(1 + \tanh(r/a))] \quad (8)$$

and

$$C_{\alpha i} = 0.5[C_{\alpha i}^{reactant}(1 - \tanh(r/a)) + C_{\alpha i}^{product}(1 + \tanh(r/a))] \quad (9)$$

where again r is the position of the hydrogen atom relative to a specified point along the A1−B1 bond. The parameter a is the same as in eq 6. The geometry of the transition state is not explicitly calculated and is determined instead by our switching algorithm.

The potential energy surface described in this paper has many fundamental similarities to the empirical valence bond (EVB) formalism developed by Warshel and co-workers.[16] In the EVB formalism, a reaction is represented in terms of valence bond structures, and the ground state is obtained by mixing these structures (i.e. by diagonalizing the EVB Hamiltonian). The EVB Hamiltonian is constructed from diagonal elements that describe the energies of the different resonance structures (and which include the interaction between the solute and the solvent) and off-diagonal elements that describe the coupling between the different resonance structures (and which are independent of solvent effects). Thus, the off-diagonal elements in the EVB method can be viewed as playing a similar role as the switching functions in our formalism. The EVB method differs from our method, however, in that the solvent also plays a role in determining the mixture of resonance structures. Moreover, the EVB method includes nonbonding and Coulombic interactions within the solute, and the solute atoms are not constrained. In contrast, in our method the structures of the reactant and product states are determined from *ab initio* calculations and are incorporated in the potential surface through a combination of constraint dynamics and switching functions. These constraints will be critical for the quantum dynamical simulations of hydride transfer in which only the transferring hydride will be treated quantum mechanically. In this case, the constraints will prevent nonphysical coupling between the motion of the quantum hydrogen and the vibrational modes of the classical hydrogen atoms. These constraints also allow a larger classical time step to be used for the molecular dynamics simulations.

C. Calculation of Parameters for Potential. The reaction of interest is the hydride transfer reaction from ethanol to an NAD^+ analog (specifically 1-methyl-nicotinamide) in acetonitrile and in water. The acetonitrile solvent (CH_3CN) is modeled as a rigid, linear, three-site molecule with parameters obtained from ref 51. The aqueous solvent is modeled as rigid, three-site molecules with parameters obtained from ref 52. The Lennard-Jones parameters associated with the solute atoms are those given in ref 2. The simulations were run at a temperature of 300 K. For our simulations the simulation box was a cube with sides of length 30.0 Å containing the solute and 894 water molecules or 308 acetonitrile molecules (chosen to give the experimentally determined densities at 300 K).[51,53] The Lennard-Jones and Coulombic potentials were smoothly truncated (as described in ref 14) at $R_c = 14.9$ Å. The designated switching atom for the solvent molecules was chosen to be the oxygen atom and the cyano carbon atom for water and acetonitrile, respectively. The designated switching atom for the solute was chosen to be the C3 atom of the pyridine ring, which is the carbon atom connected to the amide sidearm. This designation, together with the geometry constraints on the solute, ensures that all atoms of the solute have an adequate sphere of interaction with the solvent.

In order to obtain the parameters in the double Morse potential (eq 5), we performed *ab initio* Hartree−Fock geometry optimizations with a 6-31G* basis set[54] on the NADH analog and on the ethanol. The frequencies were determined to be 2834 and 2856 cm^{-1} for ethanol and 1-methyl-1,4-dihydronicotinamide, respectively, including the prescribed Hartree−Fock scaling factor of 0.89(29).[55] The equilibrium C−H bond lengths were determined to be 1.088 and 1.087 Å. For the dissociation energies, we used the experimentally determined value of 103 kcal/mol for general C−H bonds.[56] The parameter C was chosen to reproduce the energy difference between the reactant and product complexes obtained from *ab initio* calculations described below.

In order to obtain the charge distributions, structures, and energies of the reactant and product complexes, we performed *ab initio* Hartree−Fock geometry optimization calculations with a 6-31G* basis set[54] on a number of different forms of the complex. In our initial Hartree−Fock optimizations, we constrained R_{AH} and R_{BH} (i.e. the C−H bond lengths) to be 1.10 and 1.65 Å, respectively, for the reactant, and the reverse for the product. (These values are based on previous studies by Clark and co-workers.[38]) Moreover, in our initial studies we are assuming that the A1−B1 distance (i.e. the C−C distance) is fixed during the reaction and that the hydrogen atom lies along the C−C bond axis (i.e. the hydrogen moves in one dimension). As discussed below, these constraints will be removed in future simulations. In the reactant and product complexes obtained from the Hartree−Fock optimizations, typically the hydrogen atom is very close to the C−C bond axis and the C−C distance is similar in the reactant and product complexes. In order to account for any discrepancies, we are translating the reactant complex so that the C−C distance matches that in the product complex, and we are placing the hydrogen atom along the C−C bond axis with the appropriate C−H covalent bond length for both the reactant and product complexes. We have found that these minor alterations do not significantly affect our results. Finally, we are implementing the CHELPG method[50] to determine the partial charges for these complexes.

We emphasize that the solvent is expected to significantly affect the structures and charge distributions of the solute. In particular, the solvent may disrupt hydrogen bonds that form within the gas phase solute molecules. Although we are neglecting these solvent effects for the simulations in this paper, these effects can be incorporated in a variety of ways. For example, self-consistent reaction field (SCRF) methods,[55] which treat the solvent as a continuum of uniform dielectric constant, could be used to obtain the reactant and product solute structures. We applied both the Onsager and the self-consistent isodensity polarized contiuum model (SCIPCM) implementations of SCRF[55] to the *trans* deprotonated form and found that the complex geometry did not change significantly with these methods. Another approach would be to obtain the reactant and product solute structures from *ab initio* calculations on supermolecules consisting of the solute and several solvent molecules. Alternatively, the reactant and product solute structures and charge distributions could be obtained from simulations in solution using standard molecular mechanical force fields. These are directions for future research.

D. Classical Free Energy Calculations. In order to study the solvent effects for hydride transfer reactions, we are calculating the classical free energy curves for a series of model systems using the following approximate expression for the classical potential of mean force[17]

$$W(R_{AB}^{\circ}, r) \approx V_{HB}(R_{AB}^{\circ}, r) - \int_{r_0}^{r} dr' \langle F_r^S(R_{AB}^{\circ}, r') \rangle \quad (10)$$

where R_{AB}° represents a fixed distance between the atoms A1 and B1 (i.e. a fixed C−C distance), r represents the position of the hydrogen atom relative to the midpoint of the A1−B1 (C−C) bond axis, r_0 is an arbitrary reference position, $V_{HB}(R_{AB}^{\circ}, r)$ represents the interactions within the AH−B complex, and $\langle F_r^S(R_{AB}^{\circ}, r') \rangle$ indicates an average of the solvent forces on coordinate r performed with the constraints $r = r'$ and $R = R_{AB}^{\circ}$. These average forces are obtained by performing classical molecular dynamics simulations with constraints $R = R_{AB}^{\circ}$ and $r = r'$ and using a finite-difference method to calculate the forces on r. For the simulations presented in this paper, these forces

were averaged over 10 ps. The resulting curve is an average curve since solvent fluctuations will continually change its shape. Moreover, the quantum mechanical behavior of the hydrogen atom is not included in these classical free energy calculations. Nevertheless, comparison of the gas phase potential curves and the classical free energy curves illustrates the energetic effects of the solvent.

E. Calculations of Hydrogen Bonding between Solvent and Solute. The importance of hydrogen bonding (both intra- and intermolecular) and its effect on structure and reactivity of biological molecules has long been recognized. We implement the methodology used by Meng and Kollman for studying the properties of water around simple organic solutes[46] to study hydrogen bonding between the aqueous solvent and the solute for our system. In order to study the interactions of water with different atoms in the solute, we calculate radial distribution functions between specified solute atoms and water atoms. The solute atoms of particular interest for the current complexes are the oxygen of the substrate, the carbonyl oxygen of the NADH amide sidearm, and, in the protonated species, the hydrogen on the substrate oxygen. In order to further study hydrogen-bonding interactions between water and specific solute atoms, we calculate the orientational distributions of the hydration shell water molecules around designated solute atoms. A zone is defined around each of the designated solute atoms, and a water molecule is considered to inhabit a certain zone if the distance between the oxygen of the water and the center of the zone (defined to be the coordinates of the designated atom) is less than some cutoff distance r_c and if the oxygen lies closer to that zone center than to any other (i.e. a water may inhabit at most one zone). Information on the hydrogen bonding between the solvent and solute can be obtained from the orientational distribution of hydration shell waters with respect to zone centers. This orientational distribution is presented in terms of the angle θ, defined as the angle between the permanent dipole axis of water and the vector from the oxygen of the water to the zone center. As discussed in ref 46, for H-bond-donating orientations of the water this angle is 45−65°, and for H-bond-accepting orientations of the water this angle is 130−150°. In our simulations these orientational distribution curves were averaged over 16 individual 10 ps runs. This hydrogen-bonding analysis provides insight into the detailed solvent−solute interactions and elucidates the classical free energy curves.

III. Results

A. Structures and Charge Distributions of Complexes. In this section we present the structures and charge distributions of the reactant and product NADH−substrate complexes obtained from the gas phase *ab initio* Hartree−Fock geometry optimizations. (The details of these calculations are described in section II.C.)

Several issues must be addressed in calculating structures for these complexes. The first is the orientation of the amide sidearm on the NADH analog. We use the notation *cis* or *trans* to indicate that the carbonyl oxygen of the amide sidearm on the NADH analog is *cis* or *trans* to C2 of the pyridine ring. This issue has been addressed in a number of theoretical studies. Houk and co-workers have performed a series of MP2/6-31G* calculations on *cis* and *trans* conformers of nicotinamide and 1,4-dihydronicotinamide, finding the *cis* conformer to be ≈ 1 kcal/mol lower in energy than the *trans* for both species.[26] Gready and co-workers performed SCF/6-31G calculations on 1-methyl-nicotinamide and 1-methyl-1,4-dihydronicotinamide and found the *cis* conformers to be 3−4 kcal/mol lower.[29] However, the *trans* conformation is the form more frequently observed in crystal structures of the enzyme-bound cofactor.[33] Several independent theoretical studies indicate a low energetic barrier to sidearm rotation (*cis/trans* interconversion) in the uncomplexed state.[24,26,29] The *cis* and *trans* conformers demonstrate markedly different internal hydrogen bonding, which has been shown to play an important role in reactions of this type.[24,30] Thus we perform calculations on both *cis* and *trans* conformations of the product and reactant states.

Another structural issue to be addressed is the protonation of the substrate in the complex. We use the notation protonated and deprotonated to indicate the presence or absence of a proton on the oxygen of the substrate. Since protonation will significantly affect the internal hydrogen bonding, this issue also must be explored. As indicated in Figure 1, the NADH hydride transfer reaction involves the deprotonation of the alcohol. The order in which the hydride transfer and deprotonation reactions occur is a complex issue.[31,33,57] The structural and energetic effects of deprotonation have been studied previously with semiempirical molecular orbital methods to determine transition state structures in the gas phase for both the protonated and deprotonated substrate.[31,33] However, solvent effects are expected to significantly alter the energetics of these reactions. We have therefore accumulated results for both protonated and deprotonated forms of the complex. Note that another factor that is expected to affect the relation between the hydride transfer and the alcohol deprotonation is the presence of a metal ion catalyst, since the alcohol is expected to be complexed to the metal in the form an alkoxide ion.[38,58] In this paper we do not include such a metal ion catalyst, but this is a direction for future work.

Thus calculations have been performed on four variants of the NADH−substrate complex: *trans* protonated, *trans* deprotonated, *cis* protonated, and *cis* deprotonated. The *trans* deprotonated case was found to give a highly warped structure which we consider to be an artifact of calculating the structure in the gas phase (i.e. the negatively charged oxygen atom in the alkoxide ion is highly unstable). As a result the *trans* deprotonated case is left to future work where solvent and/or metal catalyst effects are included in obtaining the structures of the complex. Figures 2−4 depict the structures for the remaining three cases.

In order to present the current work in context, we compare some of the structural details of our results to those found in previous studies. The effect of nicotinamide ring puckering in NADH has been a topic of discussion for more than a decade. A survey of *ab initio*[25−27] semiempirical,[28,33] molecular mechanical,[33] and X-ray crystallographic data[33] indicates a preference for a quasi-boat-like configuration. The trend is for the C4 (i.e. the active carbon atom) to bend out of the plane of the ring by 0−15° in the direction of the transferring hydrogen and for the nicotinamide nitrogen to bend by a smaller amount. We have found our structures to match these results, with the C4 bending out-of-plane by 3−10°, and the nicotinamide nitrogen bending out-of-plane by 1−7°. In all cases the nicotinamide nitrogen bends by a smaller or equivalent amount as the C4. In addition, semiempirical and *ab initio* calculations,[24,26,27,30] as well as the experimental work of Ohno,[59,60] suggest a propensity for the amide sidearm to rotate out-of-plane in the direction of the transferring hydride. Deng and co-workers[28] have found the orientation of the amide sidearm to have a small energetic effect. We have found the amide sidearm to tilt toward the transferring hydride by 5−30°, with the exception of the reactant form of the *cis* protonated conformer, where the tilt is in the opposite direction by 10°. Furthermore, our CHELPG charge calculations show the carbonyl group of the NADH amide

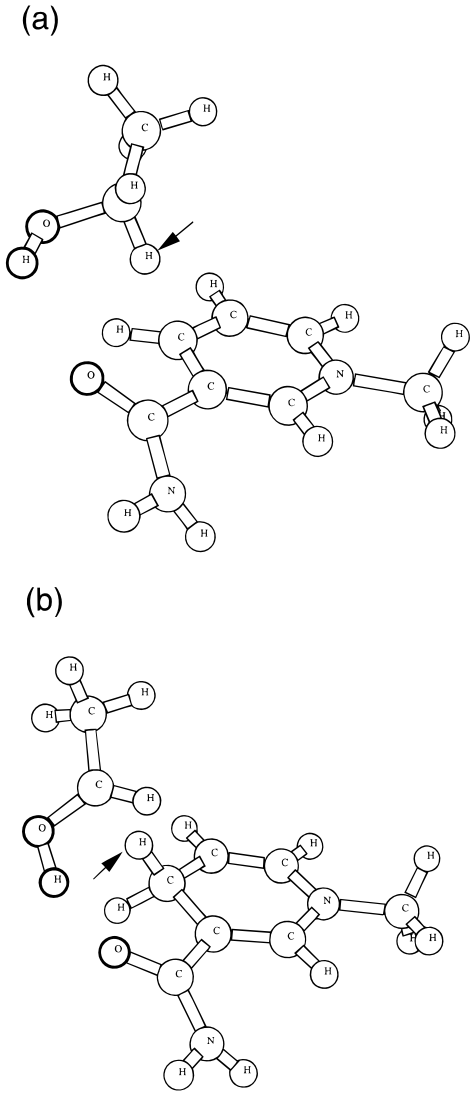

Figure 2. Structure of the *trans* protonated complex: (a) reactant and (b) product. The arrow indicates the transferring hydride. The thicker circles indicate the designated atoms for the hydrogen-bonding results in subsequent figures.

TABLE 1: Charges on Representative Solute Atoms

solute atom		*trans* prot	*cis* deprot	*cis* prot
ethanol substrate oxygen	reactant	−0.7207	−0.9102	−0.7399
	product	−0.5325	−0.5840	−0.5287
ethanol substrate hydroxyl proton	reactant	0.4590		0.4650
	product	0.5326		0.4981
transferring hydride	reactant	−0.0805	−0.1538	−0.0300
	product	−0.2524	−0.2501	−0.2350
NADH sidearm carbonyl oxygen	reactant	−0.6056	−0.7026	−0.6079
	product	−0.7496	−0.6780	−0.6015
NADH sidearm carbonyl carbon	reactant	0.8976	0.9295	0.8784
	product	0.9917	0.9273	0.8666
NADH sidearm (total)	reactant	0.1614	0.0981	0.1359
	product	0.1173	0.0621	0.0971

sidearm to be highly charged, in accordance with the the results of Donkersloot and Buck.[24] Charges on representative atoms are shown in Table 1. Another important structural issue is the C−H−C angle (i.e. the angle between the donating carbon atom, the transferring hydride, and the accepting carbon atom). The calculations of Bodor, Brewster, and Kaminski[23] indicate a linear C−H−C angle in the transition state, while others suggest it should be slightly bent.[13,30] Bodor, Brewster, and Kaminski have further suggested that a bend in the C−H−C angle by 30° or less is energetically negligible.[23] We have found the C−H−C angle to be 151−172° (with the exception of the

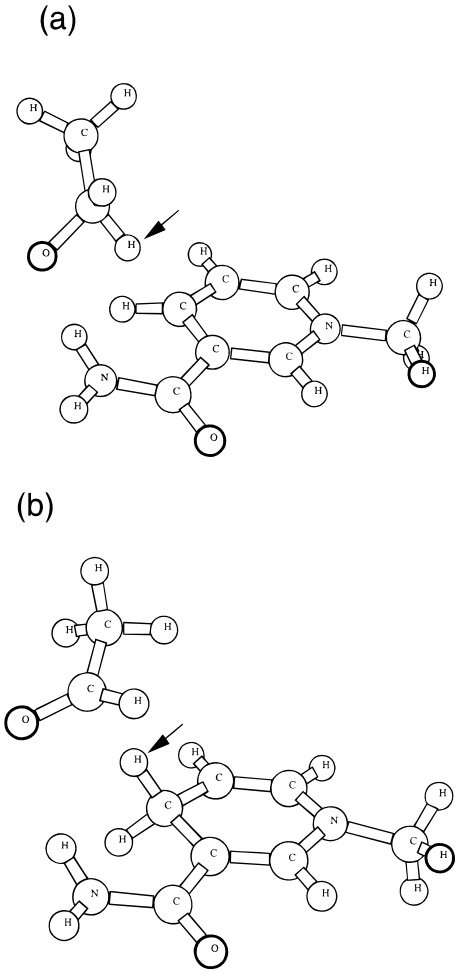

Figure 3. Structure of the *cis* deprotonated complex: (a) reactant and (b) product. The arrow indicates the transferring hydride. The thicker circles indicate the designated atoms for the hydrogen-bonding results in subsequent figures.

reactant form of the *cis* deprotonated form, which has an angle of ∼137°). As discussed in section IIB, however, for computational convenience we assume that the hydride moves in one dimension (i.e. that the C−H−C angle is linear).

The variation in internal hydrogen bonding between the different cases (*trans* protonated, *cis* protonated, and *cis* deprotonated) is clearly seen in Figures 2−4. In the *trans* protonated system (Figure 2), the proton on the substrate is clearly hydrogen bonding to the carbonyl oxygen of the NADH amide sidearm. The distance between the substrate oxygen and the sidearm oxygen is 3.00 and 2.53 Å in the reactant and product states, respectively. Thus the hydrogen bond is stronger in the product state, which correlates with the larger positive charge on the substrate proton in the product state, as shown in Table 1. This hydrogen bonding stabilizes the structure through formation of an effective eight-membered ring, which is highly reminiscent of the semiempirical AM1 results of Almarsson and Bruice.[33] We have found the reactant state to be more stable by 16.5 kcal/mol. This is due to the more stable charge distribution when the NAD^+ moiety has a formal charge of +1, as compared to the product state when the substrate has a formal charge of +1. Almarsson and Bruice found the reactant state to be lower in energy by 24 kcal/mol for a similar complex involving a methanol (formaldehyde) substrate.[33]

In the *cis* deprotonated case (Figure 3), the substrate oxygen is a hydrogen bond acceptor for one of the NADH sidearm amide hydrogens. The distance between the substrate oxygen and the amide nitrogen is 2.79 and 3.20 Å in the reactant and

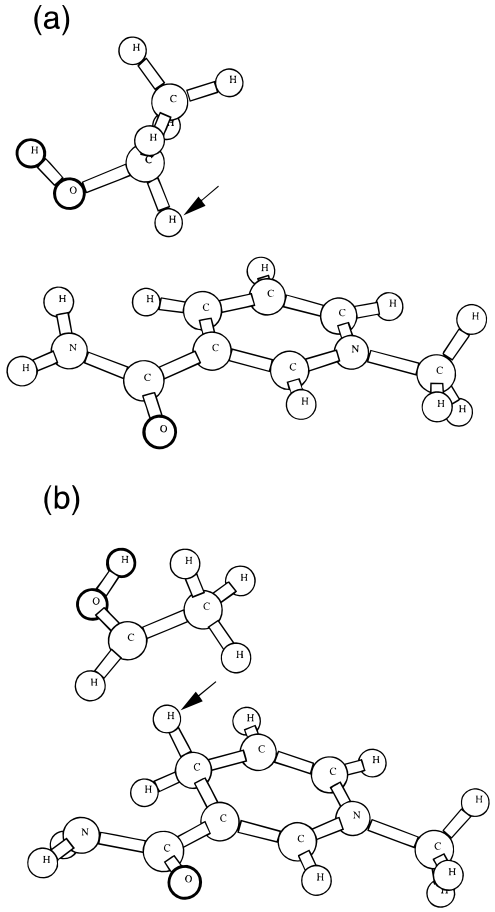

Figure 4. Structure of the *cis* protonated complex: (a) reactant and (b) product. The arrow indicates the transferring hydride. The thicker circles indicate the designated atoms for the hydrogen-bonding results in subsequent figures.

product states, respectively. In this case the hydrogen bond is stronger in the reactant state, which correlates with the larger negative charge on the substrate oxygen in the reactant state, as shown in Table 1. We have found the product state to be more stable by 41 kcal/mol using RHF/6-31G*, which is due to the instability of the alkoxide ion. Almarsson and Bruice found the product state to be lower in energy by 50 kcal/mol for a similar complex involving a methanol (formaldehyde) substrate.[33]

In the *cis* protonated form (Figure 4) a hydrogen bond between the substrate oxygen and one of the NADH sidearm amide hydrogens is present in the reactant state (where the distance between the substrate oxygen and the sidearm nitrogen is 3.07 Å), but no internal hydrogen bonding is exhibited in the product state, where the substrate oxygen twists away from the carbonyl sidearm. Note that the substrate oxygen is significantly more negative in the reactant state, as shown in Table 1. As in the *trans* protonated case, the reactant state is more stable due to a preference for a formal positive charge on the nicotinamide. In this case the reactant state is more stable by 40 kcal/mol (as opposed to 16.5 kcal/mol for the *trans* protonated form) due to the absence of hydrogen bonding in the product state in this case (compared to the stronger hydrogen bonding in the product state than in the reactant state for the *trans* protonated form).

B. Classical Free Energy Curves. Figure 5 depicts the gas phase potential curves and the classical free energy curves in acetonitrile and in water for the conformations shown in Figures 2−4. As discussed in the previous section, we have found that the reactant complex is more stable than the product complex in the gas phase for the protonated substrate (Figures 2 and 4),

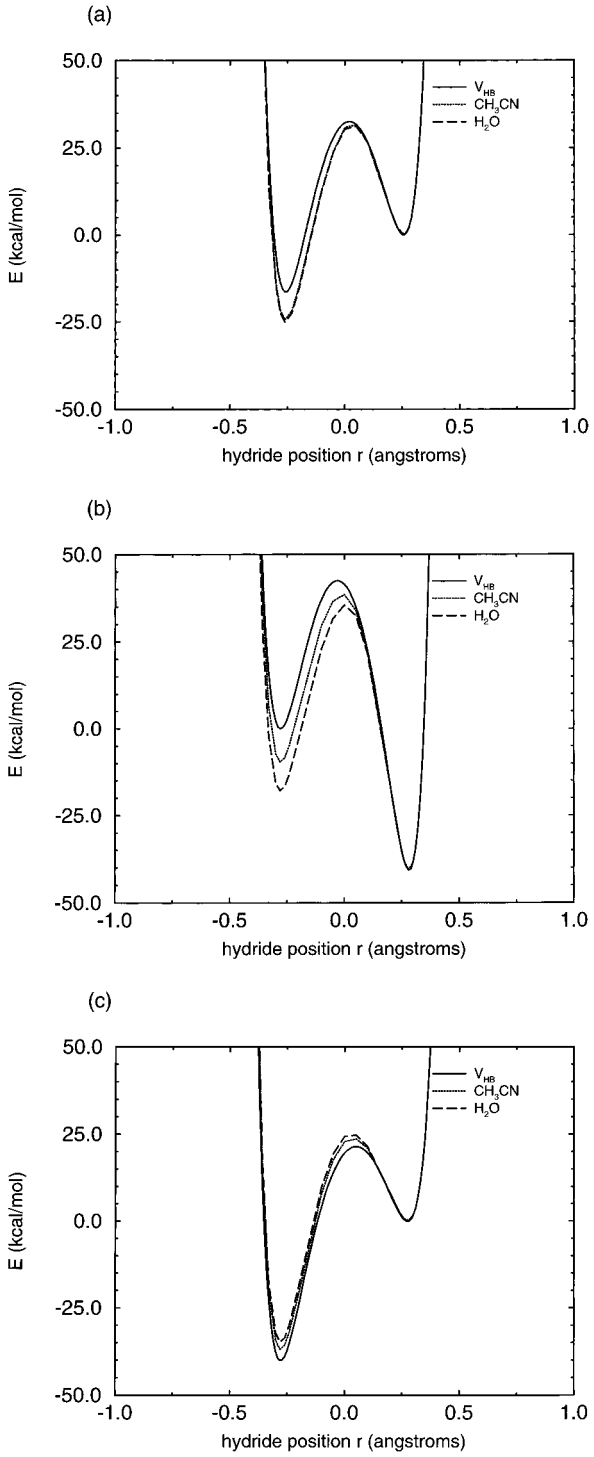

Figure 5. Gas phase potential energy curve (solid) and the classical free energy curve in water (long dashes) and in acetonitrile (short dashes) as a function of the position of the transferring hydride: (a) *trans* protonated, (b) *cis* deprotonated, and (c) *cis* protonated.

whereas the product complex is more stable than the reactant complex in the gas phase for the deprotonated substrate (Figure 3). The species with the larger dipole moment is expected to be more stabilized by polar solvents such as water and acetonitrile. This effect is seen for the *cis* deprotonated form (Figure 5b), where the solvent stabilizes the reactant form more than the product form, and Gaussian 94[54] predicts a dipole moment of ≈5.93 D for the product and ≈ 12.50 D for the reactant. We do not report dipole moments for the protonated forms of the complex since the dipole moment will depend on the choice of origin for charged species. In both the *trans* protonated (Figure 5a) and the *cis* deprotonated (Figure 5b)

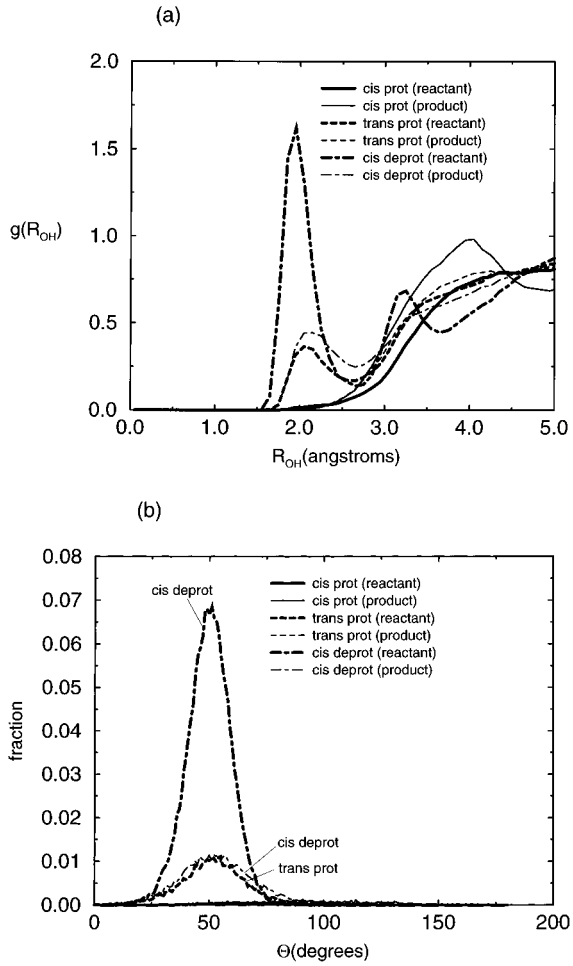

Figure 6. Hydrogen bonding between the substrate oxygen atom and the water solvent: (a) the radial distribution function between the substrate oxygen atom of the solute and the hydrogen atoms of the water; (b) the orientational distribution of hydration shell waters with respect to the substrate oxygen atom of the solute. The reactant curves are indicated with thick lines, and the product curves are indicated with thin lines. The *cis* protonated curves are indicated with solid lines, the *trans* protonated curves are indicated with dashed lines, and the *cis* deprotonated curves are indicated with alternating dashes and dots.

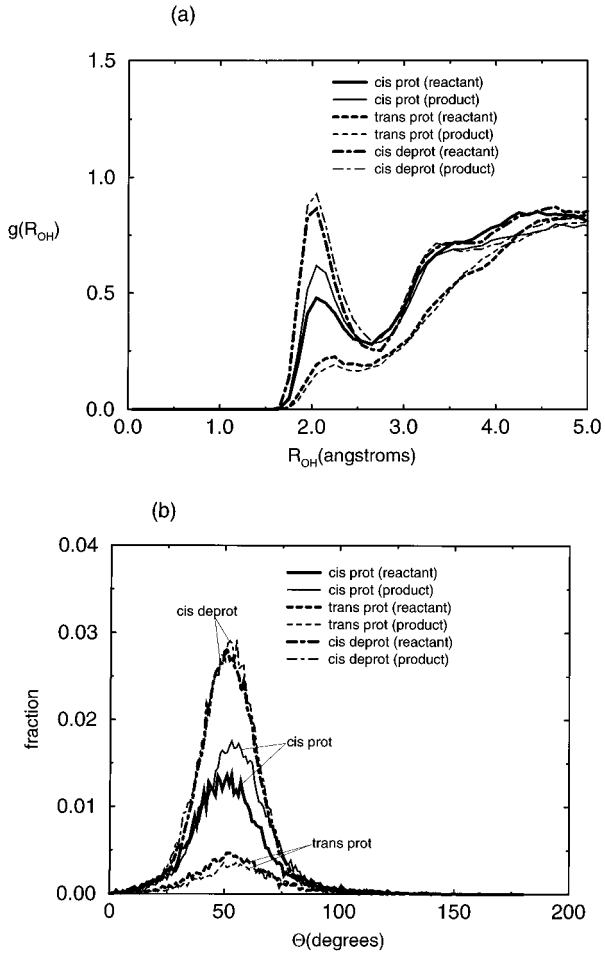

Figure 7. Hydrogen bonding between the NADH amide sidearm carbonyl oxygen atom and the water solvent: (a) the radial distribution function between the sidearm oxygen atom of the solute and the hydrogen atoms of the water; (b) the orientational distribution of hydration shell waters with respect to the sidearm oxygen atom of the solute. The reactant curves are indicated with thick lines, and the product curves are indicated with thin lines. The *cis* protonated curves are indicated with solid lines, the *trans* protonated curves are indicated with dashed lines, and the *cis* deprotonated curves are indicated with alternating dashes and dots.

forms of the complex, the solvent stabilizes the reactant state more than the product state, thus decreasing the energy gap between reactants and products for the *cis* deprotonated form and increasing the gap for the *trans* protonated form. The *cis* protonated form (Figure 5c) differs from the other two cases in that calculated solvent effects predict stabilization of the product well relative to the reactant well. This decreases the energy gap between product and reactant states, although the magnitude is smaller than that seen in the other two cases. The differences among these free energy curves will be explained through the hydrogen bonding analysis in section III.C.

Note that in all three cases, the calculated solvent effects are greater for water than acetonitrile. This is due in part to the difference in dielectric constants: water and acetonitrile have dielectric constants of 78.5 and 38.8, respectively, at 300 K.[53,61] In addition, as will be discussed in the next section, hydrogen-bonding effects between the solvent and solute play an important role in determining the shapes of these free energy curves. Water can function well as both a hydrogen bond acceptor and a hydrogen bond donor. In contrast, while acetonitrile may function as a hydrogen bond acceptor it is expected to function poorly as a hydrogen bond donor.

C. Hydrogen Bonding between Solvent and Complex. Figures 6−8 depict the radial distribution functions between designated atoms in the solute and water and the orientational distributions of water molecules in zones around designated atoms in the solute. The designated atoms are chosen to be the substrate oxygen, the carbonyl oxygen of the NADH amide sidearm, and, in the protonated species, the hydrogen bonded to the substrate oxygen. Results are shown for both the reactant and the product forms of the complex in all three cases. (The details of the calculations are described in section II.D.)

The radial distribution functions presented in Figures 6a and 7a are between designated solute oxygen atoms and water hydrogen atoms; the radial distribution functions presented in Figure 8a are between designated solute hydrogen atoms and water oxygen atoms. In Figure 6 the designated atom is the substrate oxygen, and in Figure 7 the designated atom is the NADH amide sidearm oxygen. In Figure 8 the designated atom is the substrate hydroxyl proton for the protonated forms and is a hydrogen atom in the methyl substituent of the NADH analog for the deprotonated form. A peak at $R_{OH} < 3.0$ Å in these radial distribution functions indicates hydrogen bonding.

For the orientational distributions, the cutoff distance for the zones is chosen to be $r_c = 3.0$ Å for all designated atoms. This treatment differs slightly from the work of Meng and Kollman,[46] who chose r_c to be the first minimum of the radial distibution

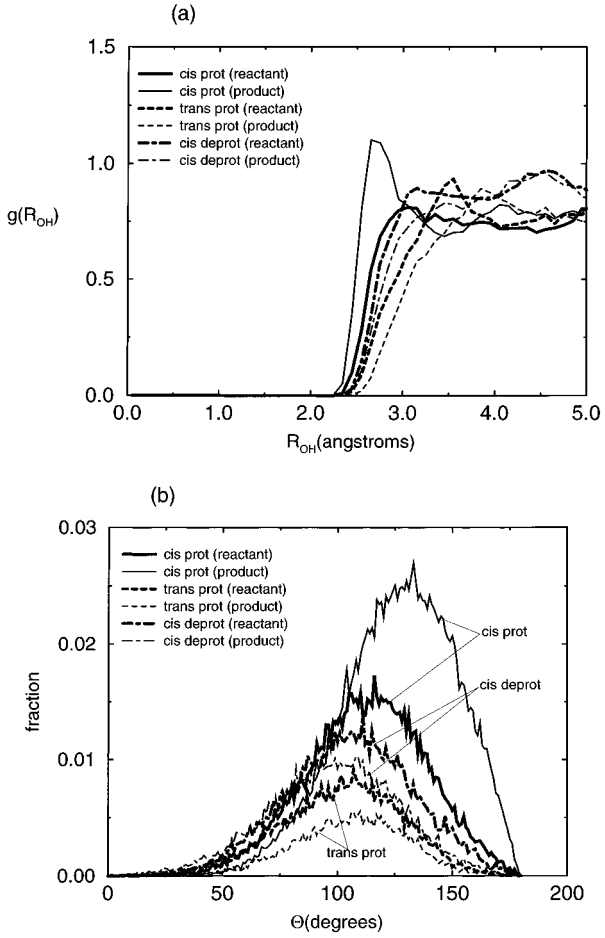

Figure 8. Hydrogen bonding between the designated hydrogen atom of the solute (the substrate hydroxyl proton for the protonated forms and a hydrogen atom in the methyl substituent of the NADH analog for the deprotonated form) and the water solvent: (a) the radial distribution function between the designated hydrogen atom of the solute and the oxygen atoms of the water; (b) the orientational distribution of hydration shell waters with respect to the designated hydrogen atom of the solute. The reactant curves are indicated with thick lines, and the product curves are indicated with thin lines. The *cis* protonated curves are indicated with solid lines, the *trans* protonated curves are indicated with dashed lines, and the *cis* deprotonated curves are indicated with alternating dashes and dots.

function. The radial distribution functions presented below indicate that the cutoff distance of $r_c = 3.0$ Å is not optimal, but it is adequate for the qualitative analysis in this paper. A quantitative analysis would require a more careful treatment of these cutoff distances. In Figures 6b and 7b the substrate oxygen and the amide carbonyl oxygen serve as hydrogen bond acceptors, as indicated by the peaks at ∼55°. In Figure 8b the proton serves as a hydrogen bond donor, as indicated by the peaks at ∼130°. As discussed in ref 46, a peak at 90−100° indicates an uncorrelated distribution. Note that in Figure 8b the methyl hydrogen atom (for the *cis* deprotonated form), which is not expected to experience significant hydrogen bonding, exhibits a peak at ∼100°.

For the *trans* protonated form, Figure 6 indicates that the substrate oxygen exhibits hydrogen bonding with water in the reactant but not in the product state, which explains the stabilization of the reactant state relative to the product state in the classical free energy curves in solution (Figure 5a). The difference in hydrogen bonding by the substrate oxygen is due mainly to the larger negative charge on the substrate oxygen for the reactant than for the product form, as shown in Table 1. Figure 8b indicates that the substrate proton does not exhibit significant hydrogen bonding with water since the data resembles an uncorrelated distribution with a peak at ∼100°. Figure 7 indicates that the degree of hydrogen bonding between the amide carbonyl oxygen and the water is similar for the reactant and product states. These peaks are substantially smaller in magnitude than in the *cis* forms of the complex due to the internal hydrogen bonding between the amide carbonyl oxygen and the substrate hydroxyl hydrogen. Note that the charge on the carbonyl oxygen is more negative for the product than for the reactant state, but the internal hydrogen bonding is weaker for the reactant than for the product state. Our results suggest that these two effects cancel each other for external hydrogen bonding.

For the *cis* deprotonated form, Figure 6 indicates that both the reactant and product states exhibit hydrogen bonding between the substrate oxygen atom and the water. However, the reactant state exhibits significantly more hydrogen bonding than the product state, which explains the stabilization of the reactant state relative to the product state in the classical free energy curves in solution (Figure 5b). This difference in hydrogen bonding can be explained by Table 1, which shows that the substrate oxygen charge is much more negative in the reactant state than in the product state. Figure 7 indicates that again the degree of hydrogen bonding between the amide sidearm carbonyl oxygen and the water is similar for the reactant and product states, which results from the similarity of the carbonyl charge and orientation in the product and reactant states.

For the *cis* protonated form, Figure 8 indicates that the degree of hydrogen bonding between the substrate proton and the water is greater in the product than in the reactant form, which explains the stabilization of the product state relative to the reactant state in the classical free energy curves in solution (Figure 5c). This difference in hydrogen bonding can be explained in part from the structures in Figure 4. In the reactant state the substrate oxygen is involved in a hydrogen bond with the sidearm amide group, which hinders accessibility of the hydroxyl group by the solvent. In contrast, in the product state the hydroxyl group of the substrate is twisted around away from the NADH and thus has more freedom to interact with the solvent. As in the previous two cases, Figure 7 indicates that the degree of hydrogen bonding between the amide carbonyl oxygen and the water is similar for the reactant and the product states, which is expected since the charge and orientation of the carbonyl do not change significantly between reactant and product states. However, note that the extent of hydrogen bonding by the sidearm oxygen is greater for the *cis* deprotonated form of the complex than for the *cis* protonated form, most likely due to the larger negative charge on the sidearm oxygen in the deprotonated case. Figure 6 indicates that the substrate oxygen does not exhibit hydrogen bonding with the solvent for both the reactant and product states. For the reactant state this lack of hydrogen bonding is most likely due to the internal hydrogen bond in the reactant form discussed above. For the product state this lack of hydrogen bonding is most likely due to the relatively small negative charge on the substrate oxygen atom, as seen in Table 1.

IV. Summary and Conclusions

We have developed an augmented molecular mechanical potential for the simulation of proton and hydride transfer reactions in solution. This potential utilizes a double Morse potential to allow specified bonds in the solute to break and form. In addition, an efficient constraint dynamics method is combined with switching functions to smoothly vary the

structure of the complex from the reactant to the product structure. Switching functions are also used to smoothly vary the atomic charges of the solute. Thus changes in hybridization, bond order, and charge distribution are incorporated into this potential. The solvent is treated explicitly in order to account for changes in hydrogen bonding between the solvent and the solute during the reaction.

We applied this method to the oxidation of ethanol by the NAD^+ analog 1-methyl-nicotinamide in acetonitrile and in water. Gas phase Hartree−Fock calculations at the 6-31G* level were performed to obtain the structures and charge distributions for the reactant and product complexes, which were used to parametrize the augmented molecular mechanical potential. Both *cis* and *trans* orientations of the NADH amide side chain and both protonated and deprotonated forms of the substrate were studied. Results from the *trans* protonated, *cis* protonated, and *cis* deprotonated forms of the complex were presented. These structures were found to display many of the same features as structures obtained in previous work, including details such as sidearm orientation, ring puckering, and internal hydrogen-bonding patterns. In general, we found that in the gas phase the reactant state was lower in energy than the product state for the protonated substrate, while the reverse was true for the deprotonated substrate. The energy gap between reactant and product states was found to vary between 16 and 40 kcal/mol, depending on the sidearm orientation and whether or not the substrate was protonated.

In order to study the effect of solvent on the energy gap between reactant and product states, we calculated the classical free energy curves in acetonitrile and aqueous solution for the hydride transfer reactions. Solvent effects were found to narrow (but not eliminate) the energy gap in the *cis* protonated and *cis* deprotonated complexes and to slightly widen the energy gap for the *trans* protonated complex. In all cases the magnitude of the change in energy gap was found to be larger for water than for acetonitrile. We also studied both the radial distribution functions between the solute and water and the orientational distribution of the hydration shell water molecules in order to elucidate the hydrogen bonding between the solvent and the solute. This hydrogen bonding was found to play an important role in the determination of the energy gap between the reactant and product states in solution.

Although the significant electronic quantum effects are incorporated in this potential energy surface, the simulations described in this paper do not include the quantum *dynamical* effects of the nuclei, such as hydrogen tunneling. However, the energy gap between reactant and product states has significant implications for the hydrogen-tunneling mechanism that requires resonance or near-resonance between the reactant and product states. We are currently using the methodology presented in this paper to simulate the quantum dynamics of NADH hydride transfer reactions. In these mixed quantum/classical molecular dynamics simulations, the hydrogen atom being transferred is treated quantum mechanically, while the remaining nuclei are treated classically. We are implementing the surface hopping method "molecular dynamics with quantum transitions" (MDQT) in order to incorporate nonadiabatic quantum dynamical effects into our simulations.[14] The kinetic isotope effects can be calculated and compared to experimental results.

The potential energy surface presented in this paper incorporates many of the fundamental chemical and physical aspects of NADH hydride transfer reactions in solution. Thus this potential energy surface should provide a qualitatively reasonable description of these reactions. In order to improve the quantitative accuracy of this potential surface, however, several additional effects must be incorporated. For example, although the charge distribution and structure of the solute are allowed to vary from the reactant to the product charge distribution as the hydride is transferred, the effect of the solvent environment on the charge distribution and structure of the solute is neglected. In particular, the solvent is expected to significantly alter the internal hydrogen bonding patterns in the solute. These solvent effects can be incorporated by obtaining the reactant and product solute structures and charge distributions from *ab initio* calculations on supermolecules consisting of the solute and several solvent molecules or, alternatively, from standard molecular mechanical simulations in solution. Moreover, specified portions of the solute, such as the NADH amide sidearm, could be allowed to move freely (i.e. to rotate and vibrate) during the reaction. This motion of the solute could be incorporated using, for example, the recently developed molecular mechanical force field for NAD^+ and NADH described in ref 62. In addition, the transition state of the complex in the gas phase could be determined from *ab initio* calculations. The energy of the transition state relative to the reactant and product states could be incorporated into the solute hydrogen-bonding potential in order to obtain a more accurate barrier, and the structure and charge distribution of the transition state could be included in the simulations through the implementation of a more complex switching function. Another important future direction is the incorporation of the vibrational motion of the donating and accepting carbon atoms into our simulations. Further future directions include the extension of our treatment of the motion of the transferring hydrogen atom to three dimensions (i.e. allowing the reactive C−H−C angle to bend rather than constraining it to remain linear) and the inclusion of polarization effects for both the solvent and the solute.

Several other important environmental effects can be incorporated into these simulations. For example, many of the NADH hydride transfer reactions in solution occur in the presence of a divalent metal ion catalyst, such as Zn^{2+} or Mg^{2+}. These metal ions are expected to play a vital role in the determination of the structure and charge distribution of the solute because they provide stabilization by complexing to the substrate oxygen atom. The effects of a divalent metal ion can be included by obtaining the reactant and product solute structures and charge distributions from *ab initio* calculations on supermolecules including a metal ion or from standard molecular mechanical simulations in the presence of a metal ion. Finally, these methods can be extended to study NADH hydride transfer reactions in enzymes such as alcohol dehydrogenases.

Acknowledgment. We are grateful to Olaf Wiest for assistance with the *ab initio* Hartree−Fock calculations. We also thank Alex Balboa and Jian-Yun Fang for useful readings of the manuscript. We acknowledge financial support from the NSF CAREER program grant CHE-9623813, the Petroleum Research Fund (administered by the ACS) grant 30432-G6, and the Clare Boothe Luce Foundation.

Appendix A. Equations of Motion for Constraint Dynamics

This appendix summarizes the derivations and results of ref 49 for easy reference. As described in section II.A, the complex of N_a atoms is divided into N_p primary atoms with $N_p(N_p - 1)/2$ bond constraints σ_{ij} of length d_{ij} and $N_s = N_a - N_p$ secondary atoms linked to the basic structure by $3N_s$ linear constraints $\boldsymbol{\tau}_\alpha$. The primary and secondary constraint equations are given in eqs 1 and 2 in section II.A, where the superscripts p refer to primary atoms and the supserscripts s refer to secondary atoms. The equations of motion for the primary

particles are

$$M_i^{(p)}\,\ddot{\mathbf{R}}_i^{(p)}(t) = \mathbf{F}_i^{(p)}(t) + \mathbf{G}_i^{(p)}(t) \tag{A1}$$

where $\mathbf{F}_i^{(p)}(t)$ is the force on coordinate $\mathbf{R}_i^{(p)}(t)$ due to intermolecular forces

$$\mathbf{F}_i^{(p)}(t) = -\nabla_i V(\mathbf{R}^{(p)}(t),\mathbf{R}^{(s)}(t)) \tag{A2}$$

and $\mathbf{G}_i^{(p)}(t)$ is the constraint force on particle $\mathbf{R}_i^{(p)}(t)$

$$\mathbf{G}_i^{(p)}(t) = -\sum_{k=1}^{N_p-1}\sum_{j=k+1}^{N_p}\lambda_{jk}(t)\,\nabla_i\sigma_{jk}(t) - \sum_{\beta=1}^{N_s}\nabla_i(\boldsymbol{\mu}_\beta(t)\cdot\boldsymbol{\tau}_\beta(t)) \tag{A3}$$

$$= -\sum_{k=1}^{N_p-1}\sum_{j=k+1}^{N_p}\lambda_{jk}(t)\,2\mathbf{R}_{jk}^{(p)}(t)(\delta_{ij}-\delta_{ik}) - \sum_{\beta=1}^{N_s}C_{\beta i}\boldsymbol{\mu}_\beta(t) \tag{A4}$$

where $\mathbf{R}_{jk}^{(p)}(t) \equiv \mathbf{R}_j^{(p)}(t) - \mathbf{R}_k^{(p)}(t)$ and $\lambda_{jk}(t)$ and $\boldsymbol{\mu}_\beta(t)$ are Lagrange multipliers. The equations of motion for the secondary particles are

$$M_\alpha^{(s)}\,\ddot{\mathbf{R}}_\alpha^{(s)}(t) = \mathbf{F}_\alpha^{(s)}(t) + \mathbf{G}_\alpha^{(s)}(t) \tag{A5}$$

where $\mathbf{F}_\alpha^{(s)}(t)$ is the force on coordinate $\mathbf{R}_\alpha^{(s)}(t)$ due to intermolecule forces and $\mathbf{G}_\alpha^{(s)}(t)$ is the constraint force on particle $\mathbf{R}_\alpha^{(s)}(t)$:

$$\mathbf{G}_\alpha^{(s)}(t) = -\sum_{\beta=1}^{N_s}\nabla_\alpha(\boldsymbol{\mu}_\beta(t)\cdot\boldsymbol{\tau}_\beta(t)) = \boldsymbol{\mu}_\alpha(t) \tag{A6}$$

Substitution of eqs A1 and A5 into the second time derivative of eq 2 leads to

$$\sum_{\beta=1}^{N_s}\boldsymbol{\mu}_\beta(t)A_{\alpha\beta} = \mathbf{T}_\alpha(t) - 2\sum_{k=1}^{N_p-1}\sum_{j=k+1}^{N_p}\lambda_{jk}(t)\,\mathbf{R}_{jk}^{(p)}(t)\,B_{jk}^{\alpha} \tag{A7}$$

where

$$A_{\alpha\beta} = \delta_{\alpha\beta}/M_\alpha^{(s)} + \sum_{i=1}^{N_p}C_{\alpha i}C_{\beta i}/M_i^{(p)} = A_{\beta\alpha} \tag{A8}$$

$$\mathbf{T}_\alpha(t) = -\mathbf{F}_\alpha^{(s)}(t)/M_\alpha^{(s)} + \sum_{i=1}^{N_p}C_{\alpha i}\mathbf{F}_i^{(p)}(t)/M_i^{(p)} \tag{A9}$$

and

$$B_{jk}^{\alpha} = C_{\alpha j}/M_j^{(p)} - C_{\alpha k}/M_k^{(p)} \tag{A10}$$

Solution of this equation for $\boldsymbol{\mu}_\alpha(t)$ and substitution into eq A1 gives

$$M_i^{(p)}\,\ddot{\mathbf{R}}_i^{(p)}(t) = F_i(t) - \sum_{k=1}^{N_p-1}\sum_{j=k+1}^{N_p}R_{jk}^{i}(t)\,\lambda_{jk}(t) \tag{A11}$$

where

$$F_i(t) = \mathbf{F}_i^{(p)}(t) - \sum_{\alpha=1}^{N_s}\sum_{\beta=1}^{N_s}C_{\alpha i}(A^{-1})_{\alpha\beta}\,\mathbf{T}_\beta(t) \tag{A12}$$

$$R_{jk}^{i}(t) = 2S_{jk}^{i}\,\mathbf{R}_{jk}^{(p)}(t) \tag{A13}$$

and

$$S_{jk}^{i} = (\delta_{ij}-\delta_{ik}) - \sum_{\alpha=1}^{N_s}\sum_{\beta=1}^{N_s}C_{\alpha i}(A^{-1})_{\alpha\beta}B_{jk}^{\beta} \tag{A14}$$

These are analogous to the equations derived in ref 49.

Appendix B. Generalized Rattle Constraint Dynamics

In this appendix we present the generalized RATTLE constraint method, which combines the method summarized in Appendix A[49] with the standard RATTLE constraint method.[48] Substitution of $\ddot{\mathbf{R}}_i^{(p)}(t)$ from eq A11 into the standard RATTLE algorithm[48] (which is based on the velocity Verlet algorithm) gives the following expressions for the coordinates and velocities at time $t + h$ (where h is the molecular dynamics time step)

$$\mathbf{R}_i^{(p)}(t+h) = \mathbf{R}_i^{(p)}(t) + h\dot{\mathbf{R}}_i^{(p)}(t) + \frac{h^2}{2M_i^{(p)}}[F_i(t) + G_i^{RR}(t)] \tag{B1}$$

and

$$\dot{\mathbf{R}}_i^{(p)}(t+h) = \dot{\mathbf{R}}_i^{(p)}(t) + \frac{h}{2M_i^{(p)}}[F_i(t) + G_i^{RR}(t) + F_i(t+h) + G_i^{RV}(t+h)] \tag{B2}$$

where

$$G_i^{RR}(t) = -\sum_{k=1}^{Np-1}\sum_{j=k+1}^{N_p}R_{jk}^{i}(t)\,\lambda_{jk}^{RR}(t) \tag{B3}$$

and

$$G_i^{RV}(t+h) = -\sum_{k=1}^{N_p-1}\sum_{j=k+1}^{N_p}R_{jk}^{i}(t+h)\,\lambda_{jk}^{RV}(t+h) \tag{B4}$$

In the RATTLE algorithm both the constraints

$$\sigma_{ij} = |\mathbf{R}_i^{(p)}(t) - \mathbf{R}_j^{(p)}(t)|^2 - d_{ij}^2 = 0 \tag{B5}$$

and the derivatives of the constraints

$$(\mathbf{R}_i^{(p)}(t) - \mathbf{R}_j^{(p)}(t))\cdot(\dot{\mathbf{R}}_i^{(p)}(t) - \dot{\mathbf{R}}_j^{(p)}(t)) = 0 \tag{B6}$$

must be satisfied.

The RATTLE algorithm consists of two separate steps. The first step is to calculate the coordinates at time $t + h$ and the velocities at time $t + h/2$. This step requires the determination of the Lagrange multipliers $\lambda_{jk}^{RR}(t)$, which are calculated iteratively. The second step is to calculate the velocities at time $t + h$. This step requires the determination of the Lagrange multipliers $\lambda_{jk}^{RV}(t+h)$, which again are calculated iteratively. The remainder of this appendix outlines these calculations.

In order to initialize the iterative loop for the first step of calculating the coordinates at time $t + h$ and the velocities at time $t + h/2$, define $\mathbf{R}_i^{T}$ to be the current approximation to $\mathbf{R}_i^{(p)}(t+h)$ and set its initial value to

$$\mathbf{R}_i^{T} = \mathbf{R}_i^{(p)}(t) + h\dot{\mathbf{R}}_i^{(p)}(t) + \frac{h^2}{2M_i^{(p)}}F_i(t) \tag{B7}$$

Also define $\dot{\mathbf{R}}_i^{T}$ to be the current approximation to

$\dot{\mathbf{R}}_i^{(p)}(t+h/2)$ and set its initial value to

$$\dot{\mathbf{R}}_i^{T} = \dot{\mathbf{R}}_i^{(p)}(t) + \frac{h}{2M_i^{(p)}} F_i(t) \tag{B8}$$

Then begin the iterative loop. Pick a constraint between atoms j and k, and let $\mathbf{R}_{jk}^{T} \equiv \mathbf{R}_j^{T} - \mathbf{R}_k^{T}$. If $|\mathbf{R}_{jk}^{T}|^2 - d_{jk}^2$ is greater than the specified tolerance, then calculate the λ_{jk}^{RR} that satisfies the constraint to first order in λ_{jk}^{RR} and change all primary coordinates and velocities accordingly

$$\mathbf{R}_i^{T} = \mathbf{R}_i^{T} - \frac{\lambda_{jk}^{RR} h^2 S_{jk}^i \mathbf{R}_{jk}^{(p)}(t)}{M_i^{(p)}} \tag{B9}$$

and

$$\dot{\mathbf{R}}_i^{T} = \dot{\mathbf{R}}_i^{T} - \frac{\lambda_{jk}^{RR} h S_{jk}^i \mathbf{R}_{jk}^{(p)}(t)}{M_i^{(p)}} \tag{B10}$$

where

$$\lambda_{jk}^{RR} = \frac{|\mathbf{R}_{jk}^{T}|^2 - d_{jk}^2}{2h\mathbf{R}_{jk}^{T}\cdot\mathbf{R}_{jk}^{(p)}(t)(S_{jk}^j/M_j^{(p)} - S_{jk}^k(t)/M_k^{(p)})} \tag{B11}$$

Now go back to the beginning of the iterative loop, choose another constraint, and continue until all the constraints are satisfied within the specified tolerance. At the end of the loop, set the primary coordinates $\mathbf{R}_i^{(p)}(t+h) = \mathbf{R}_i^{T}$ and the primary velocities $\dot{\mathbf{R}}_i^{(p)}(t+h/2) = \dot{\mathbf{R}}_i^{T}(t)$. (To reduce storage requirements, the variables $\dot{\mathbf{R}}_i^{T}$ can be stored in the same array as the variables $\dot{\mathbf{R}}_i^{(p)}$.) Calculate the secondary positions at time $t + h$ using

$$\mathbf{R}_\alpha^{(s)}(t+h) = \sum_{i=1}^{N_p} C_{\alpha i}\mathbf{R}_i^{(p)}(t+h) \tag{B12}$$

and the secondary velocities at time $t + h/2$ using

$$\dot{\mathbf{R}}_\alpha^{(s)}(t+h/2) = \sum_{i=1}^{N_p} C_{\alpha i}\dot{\mathbf{R}}_i^{(p)}(t+h/2) \tag{B13}$$

Before beginning the second step of calculating the velocities at time $t + h$, the forces $F_i(t+h)$ must be calculated for the new positions at time $t + h$. The iterative loop is initialized by defining $\dot{\mathbf{R}}_i^{T}$ to be the current approximation to $\dot{\mathbf{R}}_i^{(p)}(t+h)$ and setting its initial value to

$$\dot{\mathbf{R}}_i^{T} = \dot{\mathbf{R}}_i^{(p)}(t+h/2) + \frac{h}{2M_i^{(p)}} F_i(t+h) \tag{B14}$$

Then begin the iterative loop. Pick a constraint with atoms j and k. If $(\mathbf{R}_j^{(p)}(t+h) - \mathbf{R}_k^{(p)}(t+h))\cdot(\dot{\mathbf{R}}_j^{T} - \dot{\mathbf{R}}_k^{T})$ is greater than the specified tolerance, then calculate the λ_{jk}^{RV} that satisfies the velocity constraint by setting

$$\dot{\mathbf{R}}_i^{T} = \dot{\mathbf{R}}_i(t+h) - \frac{h\lambda_{jk}^{RV} S_{jk}^i \mathbf{R}_{jk}^{(p)}(t+h)}{M_i^{(p)}} \tag{B15}$$

where

$$\lambda_{jk}^{RV} = \frac{\mathbf{R}_{jk}^{(p)}(t+h)\cdot(\dot{\mathbf{R}}_j^{T} - \dot{\mathbf{R}}_k^{T})}{d_{jk}^2(S_{jk}^j/M_j^{(p)} - S_{jk}^k/M_k^{(p)})} \tag{B16}$$

Then return to the beginning of the velocity iterative loop, pick another constraint, and continue until all of the velocity constraints are satisfied within the specified tolerance. At the end of the loop, set the primary velocities to $\dot{\mathbf{R}}_i^{(p)}(t+h) = \dot{\mathbf{R}}_i^{T}$. (Again to reduce storage requirements, the variables $\dot{\mathbf{R}}_i^{T}$ can be stored in the same array as the variables $\dot{\mathbf{R}}_i^{(p)}$.) The secondary velocities at time $t + h$ are determined using

$$\dot{\mathbf{R}}_\alpha^{(s)}(t+h) = \sum_{i=1}^{N_p} C_{\alpha i}\dot{\mathbf{R}}_i^{(p)}(t+h) \tag{B17}$$

Note that this method differs from the standard RATTLE method[48] only by the presence of the factors S_{jk}^i. Thus if the number of secondary particles is zero (i.e. $N_s = 0$) and the resulting identities $S_{jk}^j = 1$, $S_{jk}^k = -1$, and $S_{jk}^i = 0$ for $i \neq j, k$ are substituted into the above equations, the equations for the standard RATTLE method are obtained. Note also that when the factors S_{jk}^i do not satisfy these identities (i.e. $N_s > 0$), *all* primary coordinates and velocities must be changed using eqs B9, B10, and B15 in order to satisfy a constraint between atoms j and k. In contrast, in the standard RATTLE method only the coordinates and velocities for the two atoms j and k involved in the specific constraint must be changed.

References and Notes

(1) Brooks, B. R.; Bruccoleri, R. E.; Olafson, B. D.; States, D. J.; Swaminathan, S.; Karplus, M. *J. Comput. Chem.* **1983**, *4*, 187.
(2) Cornell, W. D.; Cieplak, P.; Bayly, C. I.; Gould, I. R.; K. M. Merz, J.; Ferguson, D. M.; Spellmeyer, D. C.; Fox, T.; Caldwell, J. W.; Kollman, P. A. *J. Am. Chem. Soc.* **1995**, *117*, 5179.
(3) Chandrasekhar, J.; Smith, S. F.; Jorgensen, W. L. *J. Am. Chem. Soc.* **1985**, *107*, 154.
(4) Scheiner, S.; Duan, X. In *Modeling the Hydrogen Bond*; Smith, D., Ed.; American Chemical Society: Washington, DC, 1994; Chapter 8.
(5) Warshel, A.; Levitt, M. *J. Mol. Biol.* **1976**, *103*, 227.
(6) Singh, U.; Kollman, P. *J. Comput. Chem.* **1986**, *7*, 718.
(7) Field, M. J.; Bash, P. A.; Karplus, M. *J. Comput. Chem.* **1990**, *11*, 700.
(8) Aqvist, J.; Warshel, A. *Chem. Rev.* **1993**, *93*, 2523.
(9) Gao, J. *Acc. Chem. Res.* **1996**, *29*, 298.
(10) Cha, Y.; Murray, C. J.; Klinman, J. P. *Science* **1989**, *243*, 1325.
(11) Bahnson, B. J.; Park, D.-H.; Kim, K.; Plapp, B. V.; Klinman, J. P. *Biochemistry* **1993**, *32*, 5503.
(12) Huskey, W. P.; Schowen, R. L. *J. Am. Chem. Soc.* **1983**, *105*, 5704.
(13) Powell, M. F.; Bruice, T. C. *J. Am. Chem. Soc.* **1983**, *105*, 7139.
(14) Hammes-Schiffer, S.; Tully, J. C. *J. Chem. Phys.* **1994**, *101*, 4657.
(15) Warshel, A.; Chu, Z. T. *J. Chem. Phys.* **1990**, *93*, 4003.
(16) Warshel, A. *Computer Modeling of Chemical Reactions in Enzymes and Solutions*; John Wiley: New York, 1991.
(17) Azzouz, H.; Borgis, D. *J. Chem. Phys.* **1993**, *98*, 7361.
(18) Laria, D.; Ciccotti, G.; Ferrario, M.; Kapral, R. *J. Chem. Phys.* **1992**, *97*, 378.
(19) Staib, A.; Borgis, D.; Hynes, J. T. *J. Chem. Phys.* **1995**, *102*, 2487.
(20) Bala, P.; Grochowski, P.; Lesyng, B.; McCammon, J. A. *J. Phys. Chem.* **1996**, *100*, 2535.
(21) Lobaugh, J.; Voth, G. A. *J. Chem. Phys.* **1996**, *104*, 2056.
(22) Brewster, M. E.; Kaminski, J. J.; Huang, M.-J.; Bodor, N. *J. Org. Chem.* **1990**, *55*, 2361.
(23) Bodor, N.; Brewster, M.; Kaminski, J. J. *J. Mol. Struct.: THEOCHEM* **1990**, *206*, 315.
(24) Donkersloot, M. C. A.; Buck, H. M. *J. Am. Chem. Soc.* **1981**, *103*, 6554.
(25) Wu, Y.-D.; Houk, K. N. *J. Am. Chem. Soc.* **1991**, *113*, 2353.
(26) Wu, Y.-D.; Houk, K. N. *J. Org. Chem.* **1993**, *58*, 2043.
(27) Wu, Y.-D.; Lai, D. K. W.; Houk, K. N. *J. Am. Chem. Soc.* **1995**, *117*, 4100.
(28) Deng, H.; Zheng, J.; Sloan, D.; Burgner, J.; Callender, R. *Biochemistry* **1992**, *31*, 5085.
(29) Cummins, P. L.; Gready, J. E. *J. Mol. Struct.: THEOCHEM* **1989**, *183*, 161.
(30) Cummins, P. L.; Gready, J. E. *J. Comput. Chem.* **1990**, *11*, 791.

(31) Norris, K. E.; Gready, J. E. *J. Mol. Struct.: THEOCHEM* **1993**, *279*, 99.
(32) Ranganathan, S.; Gready, J. E. *J. Chem. Soc., Faraday Trans.* **1994**, *90*, 2047.
(33) Almarsson, O.; Bruice, T. C. *J. Am. Chem. Soc.* **1993**, *115*, 2125.
(34) Vanhommerig, S. A. M.; Meier, R. J.; Sluyterman, L. A.; Meijer, E. M. *J. Mol. Struct.: THEOCHEM* **1996**, *364*, 33.
(35) Tapia, O.; Cardenas, R.; Andrés, J.; Krechl, J.; Campillo, M.; Colonna-Cesari, F. *Int. J. Quantum Chem.* **1991**, *39*, 767.
(36) Cárdenas, R.; Andrés, J.; Krechl, J.; Campillo, M.; Tapia, O. *Int. J. Quantum Chem.* **1996**, *57*, 245.
(37) Andrés, J.; Moliner, V.; Safont, V. S.; Domingo, L. R.; Picher, M. T. *J. Org. Chem.* **1996**, *61*, 7777.
(38) von Onciul, A. R.; Clark, T. *J. Comput. Chem.* **1993**, *14*, 392.
(39) Beijer, N. A.; Buck, H. M.; Sluyterman, L. A. A.; Meijer, E. M. *Biochim. Biophys. Acta* **1990**, *1039*, 227.
(40) Olson, L. P.; Luo, J.; Almarsson, O.; Bruice, T. C. *Biochemistry* **1996**, *35*, 9782.
(41) Ho, L. L.; MacKerell, Jr., A. D.; Bash, P. A. *J. Phys. Chem.* **1996**, *100*, 4466.
(42) Kreevoy, M. M.; Ostovic, D.; Lee, I.-S. H.; Binder, D. A.; King, G. W. *J. Am. Chem. Soc.* **1988**, *110*, 524.
(43) Kim, Y.; Truhlar, D. G.; Kreevoy, M. M. *J. Am. Chem. Soc.* **1991**, *113*, 7837.
(44) Yadav, A.; Jackson, R. M.; Holbrook, J. J.; Warshel, A. *J. Am. Chem. Soc.* **1991**, *113*, 4800.
(45) Hwang, J.-K.; Chu, Z. T.; Yadav, A.; Warshel, A. *J. Phys. Chem.* **1991**, *95*, 8445.
(46) Meng, E. C.; Kollman, P. A. *J. Phys. Chem.* **1996**, *100*, 11460.
(47) Ryckaert, J.-P.; Ciccotti, G.; Berendsen, H. J. C. *J. Comput. Phys.* **1977**, *23*, 327.
(48) Andersen, H. C. *J. Comput. Phys.* **1983**, *52*, 24.
(49) Ciccotti, G.; Ferrario, M.; Ryckaert, J.-P. *Mol. Phys.* **1982**, *47*, 1253.
(50) Breneman, C. M.; Wiberg, K. B. *J. Comput. Chem.* **1990**, *11*, 361.
(51) Jorgensen, W. L.; Briggs, J. M. *Mol. Phys.* **1988**, *63*, 547.
(52) Jorgensen, W. L. *J. Am. Chem. Soc.* **1981**, *103*, 335.
(53) Weast, R. C., Ed.; *CRC Handbook of Chemistry and Physics*, 63rd ed.; CRC Press, Inc.: Boca Raton, FL, 1982.
(54) Frisch, M. J.; Trucks, G. W.; Schlegel, H. B.; Gill, P. M. W.; Johnson, B. G.; Robb, M. A.; Cheeseman, J. R.; Keith, T.; Petersson, G. A.; Montgomery, J. A.; Raghavachari, K.; Al-Laham, M. A.; Zakrzewski, V. G.; Ortiz, J. V.; Foresman, J. B.; Peng, C. Y.; Ayala, P. Y.; Chen, W.; Wong, M. W.; Andres, J. L.; Replogle, E. S.; Gomperts, R.; Martin, R. L.; Fox, D. J.; Binkley, J. S.; Defrees, D. J.; Baker, J.; Stewart, J. P.; Head-Gordon, M.; Gonzalez, C.; Pople, J. A. *Gaussian 94*, Revision B.3; Gaussian, Inc.: Pittsburgh, PA, 1995.
(55) Foresman, J. B.; Frisch, A. *Exploring Chemistry with Electronic Structure Methods*, 2nd ed.; Gaussian Inc.: Pittsburgh, PA, 1996.
(56) Eisenberg, D.; Crothers, D. *Physical Chemistry with Application to the Life Sciences*; Benjamin/Cummings: Menlo Park, CA, 1979.
(57) Andres, J.; Safont, V. S.; Martins, J. B. L.; Beltran, A.; Moliner, V. *J. Mol. Struct.: THEOCHEM* **1995**, *330*, 411.
(58) Kvassman, J.; Pettersson, G. *Eur. J. Biochem.* **1980**, *103*, 565.
(59) Ohno, A.; Kashiwagi, K.; Ishihara, Y. *Tetrahedron* **1986**, *42*, 961.
(60) Ohno, A.; Tsutsumi, A.; Kawai, Y.; Yamakazi, N.; Mikata, Y.; Okamura, M. *J. Am. Chem. Soc.* **1994**, *116*, 8133.
(61) Windholz, M., Ed. *The Merck Index*, 10th ed.; Merck & Co., Inc.: Rahway, NJ, 1983.
(62) Pavelites, J. J.; Gao, J.; Bash, P. A.; Mackerell, Jr., A. D. *J. Comput. Chem.* **1997**, *18*, 221.